Geophysical Research Letters®

Changes in the Frequency of Observed Temperature Extremes Largely Driven by a Distribution Shift

Ronak N. Patel[1] , **David B. Bonan**[1] , **and Tapio Schneider**[1]

[1]Environmental Science and Engineering, California Institute of Technology, Pasadena, CA, USA

Abstract Extreme heat poses significant threats to human life and ecosystems. Quantifying the effects of anthropogenic climate change on extreme heat has remained challenging, in part due to the short observational record. Here, we isolate the most slowly varying component of the frequency at which the historical 90th and 99th percentiles were exceeded in observational records from 1955 to 2021 by using a statistical method called low-frequency component analysis. The emerging spatiotemporal signal in the changing frequency of temperature extremes can be attributed to a shift of the temperature distribution by local warming of the annual-mean daily maximum temperature. The shift explains over 80% of the interannual variability in the frequency at which the historical 90th percentile is exceeded in the tropics and up to 50% in higher latitudes. This work connects variability in the frequency of extreme surface temperatures to variability in mean local warming.

Plain Language Summary Over the past few decades, regions across the globe have experienced substantial increases in surface temperature extremes, posing significant threats to human life, as well as critical agriculture and energy sectors. Due to the relatively short observational record, it has been difficult to disentangle the relative roles of natural variability and anthropogenic forcing in driving changes to temperature extremes. Here, we introduce a simple framework for understanding the increasing frequency of surface temperature extremes by employing a statistical method to isolate the most slowly changing, and hence most likely anthropogenic, component of surface temperature extremes. We find that the emerging signal in the changing frequency of temperature extremes is largely driven by a shift in the temperature distribution by mean local warming. The shift explains over 80% of the observed variability in exceeding the 90th percentile in the tropics and up to 50% in higher latitudes. It also explains why changes in the frequency of extremes appear to be more rapid than changes closer to the center of the temperature distribution. This work offers guidance for climate risk assessment and adaptation strategies by connecting variability in the frequency of extreme temperatures to variability in mean warming at a given location.

1. Introduction

Increasingly frequent extreme heat events pose significant threats to human health, agriculture, and energy systems worldwide (Intergovernmental Panel on Climate Change (IPCC), 2023). Distinguishing between the effects of anthropogenic climate change and natural (or internal) variability on extreme heat is crucial for effective adaptation strategies (Diffenbaugh & Field, 2013). Such differentiation has been challenging due to the relatively short observational record and regional climate variability, which exerts a strong control on local changes in extremes (Fischer & Knutti, 2014). Improving our understanding of the mechanisms driving changes in temperature extremes is essential for advancing climate resilience and informing decisions aimed at adapting to the impacts of extreme heat events in a warming climate.

Over the past decade, a series of studies have shown that changes in extreme surface temperatures over land can be related to a shift in the temperature distribution due to mean warming (e.g., Donat & Alexander, 2012; Lau & Nath, 2012; Loikith & Neelin, 2015; McKinnon et al., 2016; Rhines & Huybers, 2013; Simolo & Corti, 2022; Simolo et al., 2011; Weaver et al., 2014). For example, Donat and Alexander (2012) used global observations to demonstrate that a shift in the temperature distribution explains the rise in surface temperature extremes between two historical 30-year time periods. Similarly, Rhines and Huybers (2013) illustrated that the increased frequency of summer temperature extremes primarily reflects changes in the mean, rather than the variance, of the temperature distribution. Loikith and Neelin (2015) also show that shifting left-skewed (short right-tailed) temperature distributions to the right results in an increase in temperature extremes. Collectively, these studies show that mean local warming can explain the observed increase in temperature extremes. However, most of these studies

examine specific historical time periods (e.g., Donat & Alexander, 2012) or specific regional domains such as North America (e.g., Loikith & Neelin, 2015) or Europe (e.g., Simolo et al., 2011). It is unclear to what extent a shift of the temperature distribution in observations can explain surface temperature extremes globally and to what extent it can explain the increasing frequency of surface temperature extremes. Additionally, the short observational record and large degree of interannual-to-decadal variability have made it challenging to quantify the anthropogenic influence on observed temperature extremes.

In this paper, we introduce a framework for quantifying the spatiotemporal increase in the frequency of extreme temperatures from 1955 to 2021. We demonstrate that a shift of the temperature distribution due to mean local warming largely explains the observed increase in days surpassing historical 90th and 99th percentiles of daily maximum temperatures. This is achieved by first isolating the most slowly changing, and hence most likely forced, component of temperature extremes using a statistical method called low-frequency component (LFC) analysis (LFCA, Schneider & Held, 2001; Wills et al., 2018). By isolating the most slowly varying component in the proportion of days exceeding historical temperature thresholds, we observe a distinct difference between the increase in days above the historical 90th and 99th percentile thresholds. A slow shift in the temperature distribution by mean local warming is consistent with the more rapid acceleration in the frequency of high percentile extremes (99th percentile) compared to lower percentile thresholds (90th percentile) identified by LFCA. We then show that interannual variability in mean local warming can also explain interannual variability in the frequency of temperature extremes through a shift of the temperature distribution. While previous studies have attributed the observed increase in extreme temperatures between two historical time periods to a shift in the temperature distribution, this study comprehensively illustrates the spatiotemporal structure of these changes and connects variability in surface temperature extremes to variability in mean local warming.

2. Data and Methods

2.1. Temperature Processing

Temperature data was obtained from the Berkeley Earth Surface Temperatures data set (Rohde & Hausfather, 2020) through the gridded Experimental Global Daily Land Average High Temperature (TMAX) data set on a $1° \times 1°$ grid. Further details on the data homogenization and gridding process used in the Berkeley Earth Surface Temperatures data set can be found in Rohde et al. (2013). Even though the daily Berkeley Earth data is subject to gap-filling in the temperature reconstruction, the coarser HadGHCND observational data set (Caesar et al., 2006) is found to agree with Berkeley Earth in terms of decadal heatwave trends in regions with sufficient data (Perkins-Kirkpatrick & Lewis, 2020). This gives us confidence in the long-term trends presented by the Berkeley Earth data set.

From the provided climatology and anomaly data in the Berkeley Earth data file, we first reconstruct the observed temperature time series at each grid point from 1880 to 2021. Specifically, $T = \bar{T} - T'$ where $\bar{T}$ is the provided 1951–1980 climatology and T' is the surface temperature anomaly relative to the 1951–1980 baseline. Next, we mask out regions of the world with insufficient data, which are defined as having more than 5 days of missing data in any given year. We then subjectively determine that 1955–2021 is the period where we can maximize the portion of the world with continuous data and have the longest record possible.

Then, at each location, we calculate the 90th and 99th percentiles for the 1961–1990 baseline, which we call the "historical period." This is the first three-decade long period in the shortened time series. Finally, at each location, we compute the percent of days where the observed temperature is above the 90th and 99th percentile temperature thresholds in the historical period. This produces a spatiotemporal time series of the percent (or number) of days in a given year above the historical 90th and 99th percentile, which is later used for LFCA. To compute spatial averages of this time series, we first mask out locations with insufficient data for the period 1955–2021. From that mask, we calculate an average over each of the land regions in IPCC AR6 (Iturbide et al., 2020). Global and regional averages mentioned in the text use an area-weighted mean.

2.2. Low-Frequency Component Analysis

To estimate the spatiotemporal structure of the slow response in the frequency of extreme temperatures to climate change, we use a statistical method called LFCA (Schneider & Held, 2001; Wills et al., 2018). LFCA calculates linear combinations of a set of empirical orthogonal functions (EOFs) that maximize the ratio of low-frequency to

total variance in their corresponding time series. Those time series are called LFCs, and the combination of EOFs produces low-frequency patterns (LFPs). We define low-frequency variance as variance which makes it through a 10-year low-pass filter. Therefore, the first LFP is the linear combination of the first 15 EOFs with the highest possible ratio of interdecadal-to-intradecadal variance; that is, LFCA maximizes the ratio of multidecadal variance to higher-frequency variance to effectively isolate modes of variability with longer timescales. LFPs and LFCs are normalized such that the LFP shows the anomaly pattern corresponding to a one-standard-deviation anomaly in the corresponding LFC.

The full methodology of LFCA is given in Section 5.1 of Wills et al. (2018). The major difference between this methodology and that presented in Wills et al. (2018) is that we normalize the time series to the mean of the historical period (1961–1990), whereas Wills et al. (2018) normalizes to the mean of the entire time series. This change allows us to more easily calculate anomalies in the number of days above the historical thresholds.

2.3. Shifting the Temperature Distribution

To shift the temperature distribution at a given location by the "mean local warming," we first calculate the mean daily maximum temperature over the historical period (1961–1990). Then the annual mean daily maximum temperature for each year is calculated. From this, we obtain a mean daily maximum temperature anomaly for each year. This annual-mean anomaly provides the mean warming relative to the historical period for any specific year at any specific location and is referred to as "mean local warming."

Then, we add the annual-mean warming to the empirical cumulative density function (CDF) for the historical period at each location. Finally, we calculate the percent of this new CDF that is above the 90th and 99th percentile thresholds in the historical period. This gives us the percent of days in any year above the specified historical thresholds obtained by shifting the historical temperature distribution by the amount of warming in the mean experienced at that location. The percent of days in each year above the historical 90th and 99th percentiles is then compared to the observed incidence of those temperature extremes. To quantitatively compare the skill of the shift mechanism, we calculate the percent of variance in observed temperature extremes that is explained by a shift in the historical temperature distribution (R^2) for both the 90th and 99th percentiles.

3. Results

3.1. More Extremely Warm Days Over Time

We begin by using the Berkeley Earth Surface Temperatures data set to analyze the time series of the percent of days on which the daily maximum temperature is above the historical 90th and 99th percentiles in each of the IPCC AR6 land regions (Figure 1). Movies S1 and S2 show higher-resolution, gridded spatiotemporal changes in the percent of days above the historical thresholds from 1955 to 2021. While the number of extremely warm days has been increasing, we see large spatiotemporal variability in the trends of extreme temperatures. The relative increase in the number of days above the historical 99th percentile is greater than the increase in the number of days above the historical 90th percentile (Figure 1b). The globally averaged fractional increase from the historical period to the present is 4.5x and 2.1x for the 99th and 90th percentile thresholds, respectively. While there is substantial interannual and decadal variability in each time series, the tropical regions (Regions 9–12, 21–24, and 38), as well as North Africa (Region 20) and the Arabian peninsula (Region 36), tend to exhibit larger increases in the frequency of temperature extremes when compared to midlatitude regions, like North America (Regions 1–5), which exhibit relatively little change (Figure 1a). There also exists substantial interannual variability in the frequency of extremely warm days across all regions (Figure 1b). Next, we isolate the temporal signal present in these noisy observations across the world.

3.2. The Slowly Varying Change in Extremes

To gain insight into the spatiotemporal variability of changes in extreme temperatures, we use LFCA to extract the most slowly varying component in the percentage of days exceeding historical temperature thresholds by maximizing the ratio of low frequency to higher-frequency variance. The resulting LFCs and LFPs are interpreted in a similar way as principal components: the LFP indicates the local change associated with $\sigma = 1$ change in the LFC. The results in Figure 2 are consistent with previous studies (e.g., Hawkins et al., 2020), revealing a pronounced climate change signal in temperature extremes from the noisy underlying data set, particularly in tropical
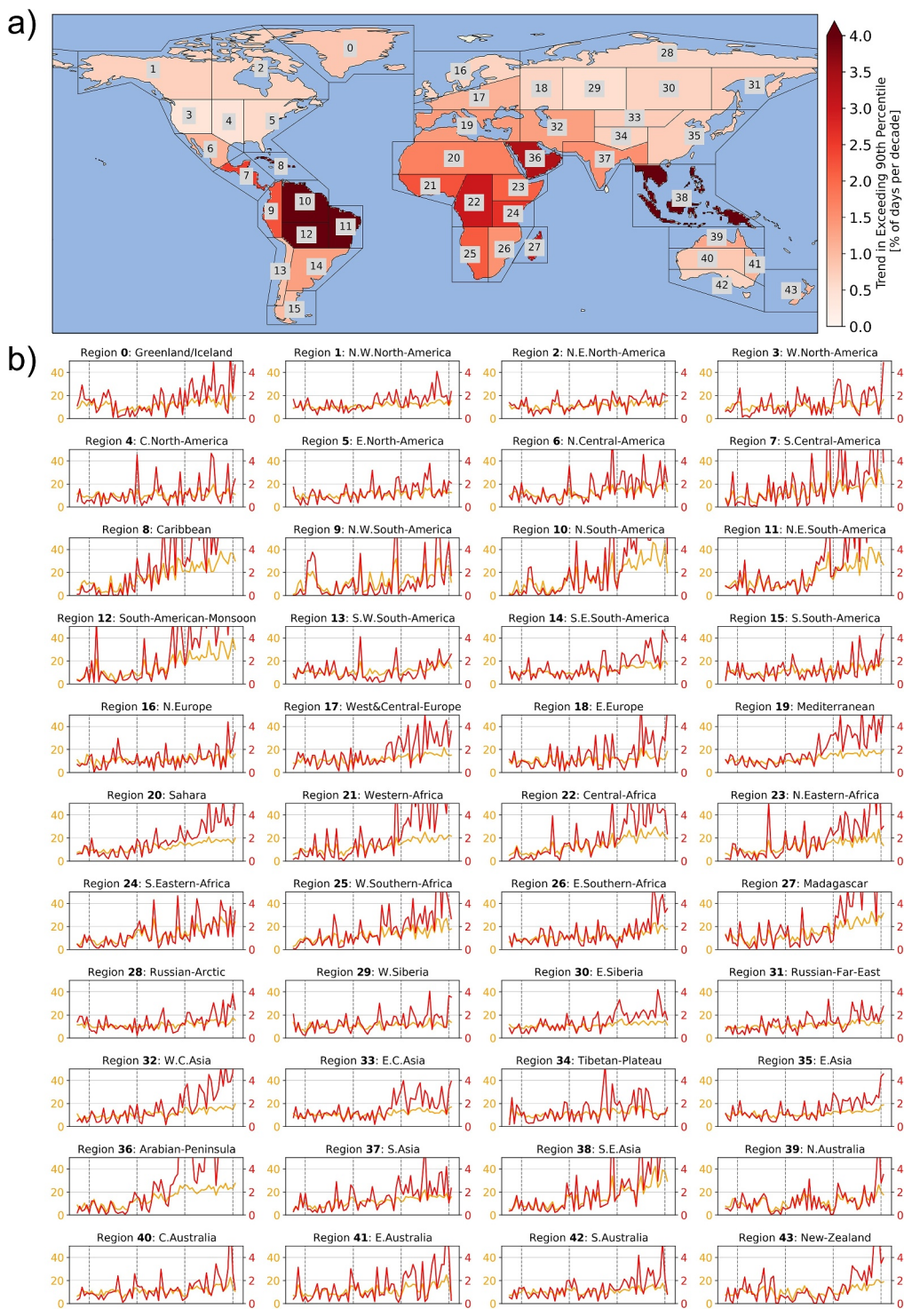
Figure 1. Observed increase in the frequency of extreme warm days from 1955 to 2021. (a) The linear trend in the percent of days in a year above the historical 90th percentile for each IPCC AR6 land region. (b) The percent of days each year from 1955 to 2021 above the historical 90th (orange) and 99th (red) percentiles in each of the IPCC AR6 land regions from panel (a). The historical period is defined as 1961–1990. The vertical gray lines in each subpanel mark every 20 years starting in 1960. Horizontal gray lines correspond to 20% and 40% of days above the historical 90th percentile. Because of the dual *y* axis, horizontal gray lines in each subpanel also correspond to 2% and 4% of days above the historical 99th percentile.
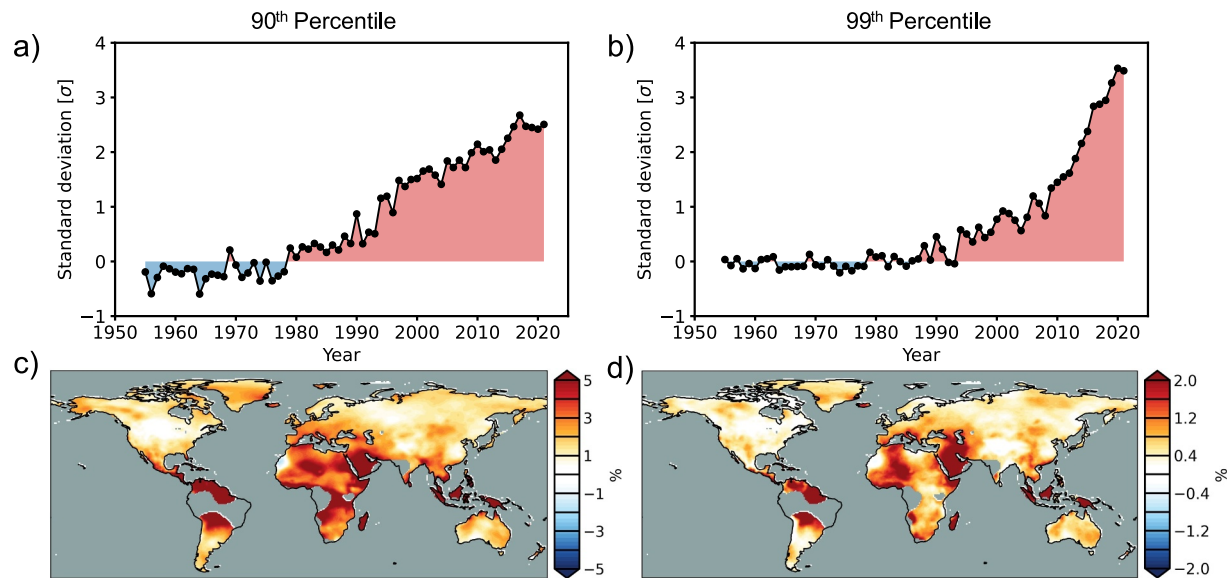
Figure 2. The slowest low-frequency components (LFCs) and corresponding low-frequency patterns (LFPs) in surface temperature extremes. The first (a) LFC and (c) corresponding LFP of the percent of days in a year where the daytime maximum temperature exceeds the historical (1961–1990) 90th percentile threshold. (b–d) Same as (a–c) but for the 99th percentile. Note different color bar limits. Locations with more than 5 days of missing data in any year from 1955 to 2021 are masked in gray.

regions where the LFP loadings are over twice as large as in the extratropics (Figures 2c and 2d). Using LFCA, we are able to effectively identify regions with the highest signal-to-noise ratio in the change in frequency of warm and extremely warm days. Increases in the frequency of temperature extremes from the historical period to 2021 across the Arabian Peninsula and North Africa are particularly prominent. There is a greater than 1.5x and 6x increase in the frequency with which the historical 90th and 99th percentile respectively are exceeded (Figures 2c and 2d). In contrast, we observe relatively little change in days above the 90th and 99th percentiles across Central North America and Western Russia (Figures 2c and 2d). The most slowly varying component of the temperature time series closely follows the observed data from Figure 1 for many of the IPCC AR6 land regions (Figure S1 in Supporting Information S1).

The spatial patterns of the change in frequency of temperature extremes are similar between the 90th and 99th percentiles (Figures 2c and 2d), which suggests a similar physical mechanism. However, the fractional increase in days above the historical 99th percentile is much larger than the 90th percentile. The temporal structure of each LFC also has a different shape. Focusing on the change in daytime temperature exceeding the historical 90th percentile (Figure 2a), the climate change signal already emerged from background variability around the year 1980, similar to the emergence in the mean (Hawkins et al., 2020). Subsequently, the percent of days exceeding the historical 90th percentile threshold increased approximately linearly. In contrast, the climate change signal in daytime temperature exceeding the historical 99th percentile emerged in the 1990s (Figure 2b), followed by a much more rapid increase in days exceeding the once-rare threshold. Many locations in the tropics and subtropics now experience a more than factor 3 increase in the frequency of this heat hazard.

3.3. Shift in the Temperature Distribution

To understand the underlying mechanism behind the spatiotemporal pattern of changes in temperature extremes isolated by LFCA, we build off previous work (e.g., Donat & Alexander, 2012; Loikith & Neelin, 2015; Rhines & Huybers, 2013) and relate the observed changes in extremes to characteristics of the temperature distribution. Tropical regions have narrower historical temperature distributions (i.e., lower standard deviation) compared to the midlatitudes (Figure S2 in Supporting Information S1). In areas where temperature distributions are narrower, warming causes a greater portion of the shifted temperature distribution to fall outside of the historical range. This results in more days in the present climate to be above a given historical extreme temperature threshold, which is why the LFP values in Figures 2c and 2d are higher in the tropics. While locations with a more negatively skewed
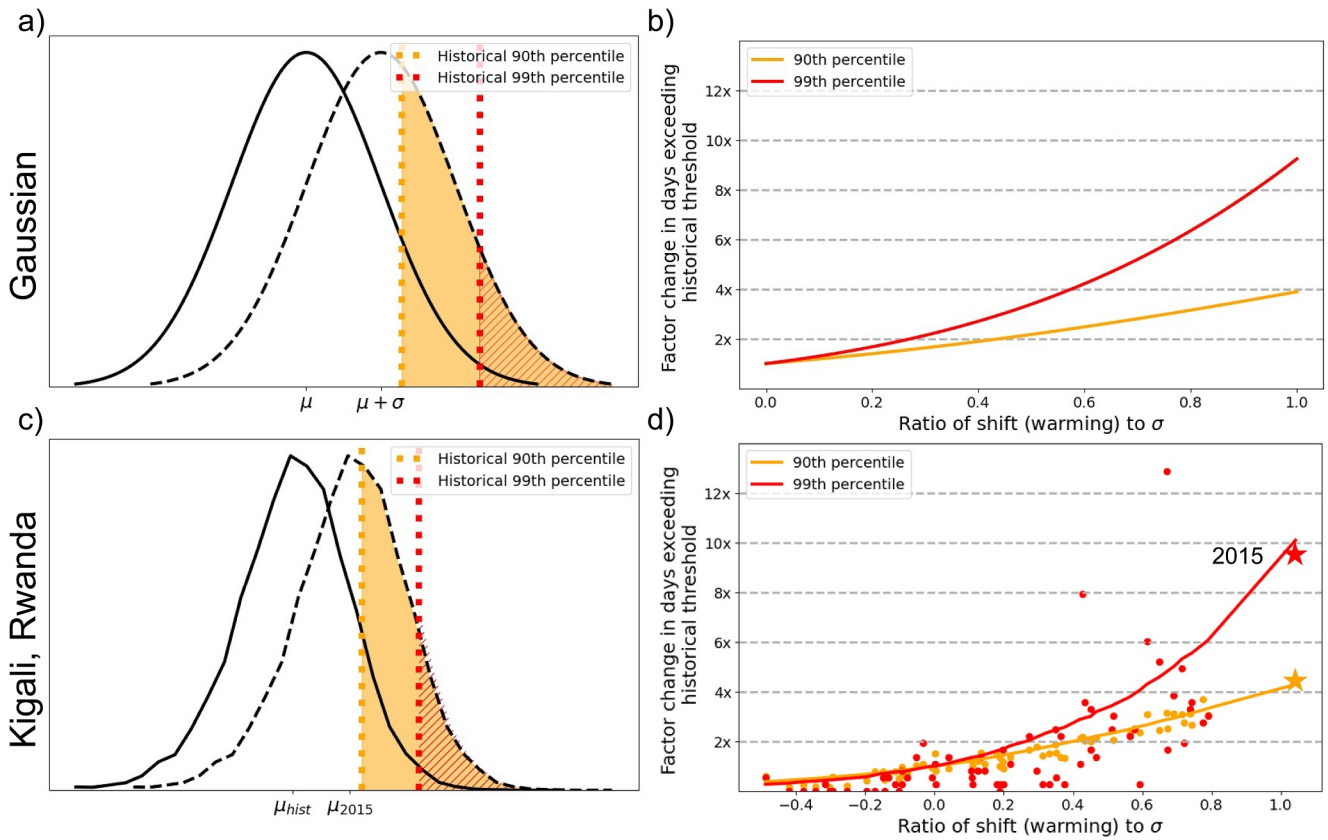
Figure 3. Shifting surface temperature distributions and the effect on changing extremes. (a) Shifting a Gaussian probability density function (PDF) with mean μ and standard deviation σ, where the solid PDF is the "historical" distribution, and the dashed PDF is the "shifted" one. Shifting a PDF causes the red hatched (days above the 99th percentile) and orange (days above the 90th percentile) areas to get larger at different rates. (b) The growing red and orange areas as a function of the shift (warming) relative to the standard deviation (width) of the distribution. (c) Shifting the historical observed temperature distribution in a tropical location (Kigali, Rwanda) by the mean temperature anomaly in 2015. (d) Same as (b) but solid lines indicate the theoretical increase in orange and red hatched area based on the distribution in panel (c). Points indicate the actual change in percent of days above historical temperature thresholds corresponding to the temperature anomaly for each year. The year 2015, corresponding to the shift in panel (c), is indicated by a star.

temperature distribution would also theoretically experience a larger fraction of days in a warmer climate falling outside of the historical range, it is much harder to pick out locations where this is the case (Figure S2 in Supporting Information S1). More negatively skewed temperature distributions along the Gulf Coast of the United States, mainland Southeast Asia, and near Paraguay are some of the few locations where this is notable (Figure S2 in Supporting Information S1 and Figures 2c and 2d).

If we approximate the annual temperature distribution at a given location as a Gaussian, the area to the right of the historical 90th and 99th percentiles will increase as we shift the distribution to the right (Figures 3a and 3b). The increase in the area to the right of the historical 90th and 99th percentile corresponds to a higher percentage of days in a year above those thresholds. The theoretical increase in the area to the right of the historical 90th and 99th percentiles qualitatively matches the temporal pattern of the increase we see in the LFCs in Figures 2a and 2b. Specifically, we would expect a more rapid increase in days exceeding the historical 99th percentile compared to the 90th, as observed. For example, in the observed temperature distribution for Kigali, Rwanda, which is approximately Gaussian, a mean shift effectively captures the changes in the 90th percentile ($R^2 = 94\%$) and qualitatively captures the changes in the 99th percentile ($R^2 = 50\%$) for any given year (Figures 3c and 3d). The temperature distribution in many locations is approximately Gaussian, which explains why the temporal patterns of LFCs in Figures 2a and 2b match so well to what is expected from shifting a Gaussian. More generally, we would see such an accelerating increase in the frequency of exceeding the historical 99th percentile for any temperature distribution $f(T)$ where $df/dT < 0$ in the neighborhood of the historical 99th percentile temperature $T = T_{99}$.
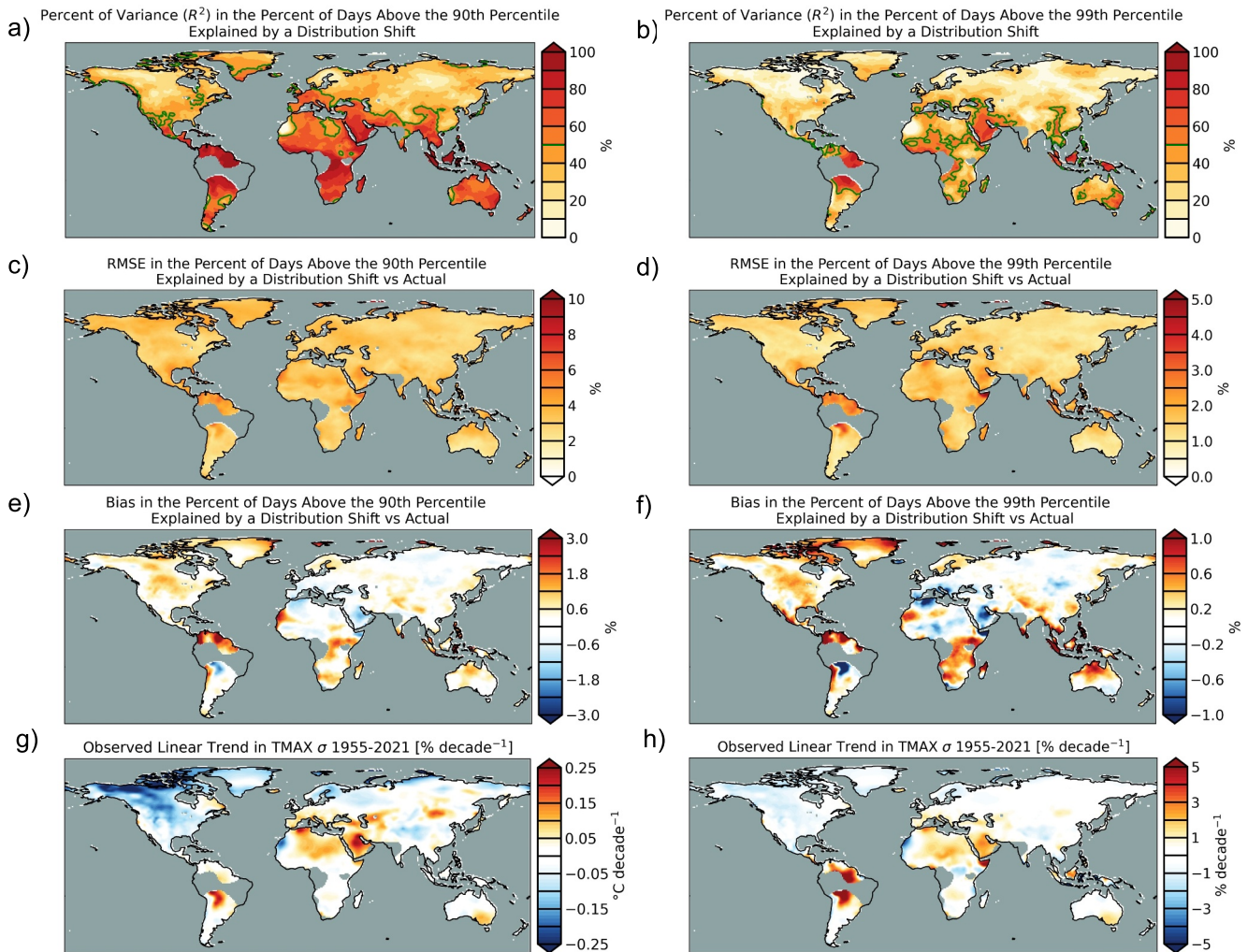
Figure 4. The square of the Pearson correlation coefficient between the expected number of days above the historical (a) 90th and (b) 99th percentiles based on a shift of the historical temperature distribution compared to the observed number of days for 1955 to 2021. The isoline of $R^2 = 50\%$ is marked in green. (c, d) Same as (a, b), but for the root mean squared error. (e, f) Same as (a, b) but for the bias of only having a distribution shift. (g) Linear least squares regression slope of the standard deviation of the annual temperature distribution from 1955 to 2021. (h) Same as (g) but normalized relative to the historical (1961–1990) standard deviation. Locations with more than 5 days of missing data in any year from 1955 to 2021 are masked in gray.

Globally, Figures 4a and 4b show the fraction of the change in frequency of exceeding the historical 90th and 99th percentiles that is explained by shifting the historical temperature distribution by the annual mean warming for every location and every year from 1955 to 2021. The shift transformation explains more than 50% of the observed variability in days above the historical 90th percentile for 55% of the land regions where we have data, including up to 80% of the variability in the tropics. The shift transformation also captures more than 50% of the changes in the more extreme 99th percentile threshold in the deep tropics, but, in that case, it becomes less accurate in the extratropics. Root mean squared errors are approximately uniform throughout the world and biases are larger for the 99th percentile threshold (Figures 4c–4f). Overall, we see that a shift of the historical temperature distribution explains most of the observed variability in the number of days above the historical extreme temperature thresholds. Using ERA5 reanalysis data (Hersbach et al., 2020) results in similar findings for the increased frequency of temperature extremes that can be explained by annual mean local warming (see Figures S3 and S4 in Supporting Information S1). Repeating this analysis by shifting the temperature distribution by the median warming relative to the historical baseline (e.g., McKinnon et al., 2024) produces comparable error in the tropics, with a lower fraction of variability in the frequency of extremes explained in the midlatitudes (Figure S5 in Supporting Information S1).

3.4. Where the Shift Mechanism Breaks Down

Shifting the temperature distribution by the mean local warming in any given year predicts much of the observed change in temperature extremes. However, there are some locations where shifting the historical temperature distribution does not match observed changes. This difference is particularly evident over North Africa, Saudi Arabia, and tropical South America (Figures 4e and 4f). Locations with a statistically significant positive bias (colored red in Figures 4e and 4f) are places where a shift of the temperature distribution by mean local warming overestimates the observed frequency of days above the 90th and/or 99th percentiles. Similarly, locations with a significant negative bias (colored blue in Figures 4e and 4f) are places where a shift of the temperature distribution underestimates the observed change in the frequency of extremes.

Shifting local temperature distributions by mean warming implicitly assumes that the moments of the distribution such as standard deviation, skewness, kurtosis, etc. remain unchanged. However, these moments can change and affect the tails of the distribution (Linz et al., 2018; Schneider et al., 2015). Linear trends in the standard deviation of the temperature distribution highlight locations experiencing changes in the width of the distribution (Figures 4g and 4h). For example, for the 90th percentile, there are large trends in the standard deviation of the temperature distribution in North America, North Africa, and Saudi Arabia (Figures 4g and 4h). Even more subtle changes of the shape of the tails, associated with higher moments of the temperature distribution such as skewness, play a larger role in temperature extremes representing the warmest few days of the year associated with the 99th percentile. For example, a trend toward more negatively skewed temperature distributions in northern Australia corresponds to an overestimate in the number of days above the historical 99th percentile (Figure 4f).

Some locations, such as the Arabian Peninsula and the Sahara Desert, have more interpolation in the Berkeley Earth data set due to the dearth of station observations there (Rohde et al., 2013). When comparing the biases presented in Figures 4e and 4f with those obtained from using ERA5 reanalysis data (Figures S4e and S4f in Supporting Information S1) we can identify locations with robust changes in temperature distributions. The trends in the standard deviation (and corresponding biases in the shift mechanism) are large in North America in both Berkeley Earth and ERA5. Additionally, both data sets show an overestimate in the number of days above the historical 90th and 99th percentile thresholds in central North America using just a shift of the temperature distribution. These are regions with dense observational networks, accounting for the correspondence between the data sets. Overall, ERA5 shows a narrowing of the temperature distribution nearly everywhere (Figures S4g and S4h in Supporting Information S1), leading to a substantial overestimate of the frequency of days above the historical 99th percentile by simply shifting the temperature distribution (Figure S4f in Supporting Information S1). Future work should examine potential causes of this global distribution-narrowing in ERA5, which is not reflected in observations.

4. Discussion and Conclusions

We have shown that the spatial pattern of changes in the frequency of temperature extremes in a given year is largely explained by a shift in the historical temperature distribution by mean local warming of that year. Using LFCA, we effectively identified regions with the highest signal-to-noise ratio in the changes in the frequency of warm and extremely warm days. Although changes in extremes, such as the frequency of days above the historical 99th percentile, are noisy, this method enabled us to extract a signal that was largely associated with a shift in the temperature distribution. While LFCA helped us capture the spatiotemporal changes in extreme temperatures, evaluating the simple shift mechanism allowed us to determine how much of the annual variability in extreme temperature frequency is linked to a mean shift (Figure 4). This mechanism provides a simple way to understand the recent observed changes in extreme temperatures. For example, due to the shape of temperature distributions (approximately Gaussian), shifting the distribution to the right over time produces an approximately exponential increase in days above the historical 99th percentile. Even a simple shift over time following mean global warming produces a perceived "acceleration" of climate change in the extremes that are of greatest social and economical consequence (Moore et al., 2019).

Previous work has shown a rapid increase in tropical temperature extremes in models (e.g., Coumou & Robinson, 2013; King et al., 2015; Perkins-Kirkpatrick & Gibson, 2017) and observations (e.g., Hawkins et al., 2020), which corroborates the results presented here. Because of their smaller temperature variance, the tropics are being pushed outside their historical temperature distribution more quickly than other regions, which has profound

implications for adaptation strategies in these vulnerable areas, particularly for the health, agriculture, ecosystem, and energy sectors. This work might also prove useful for downscaling future climate projections and regional extreme heat risk assessment by providing an effective way to generate changes in local extremes via a climate shift transformation. For the few locations experiencing significant changes to the width of the temperature distribution, the simple shift transformation can be augmented by taking into account changes in the standard deviation and, possibly, higher moments. Prior work has differed on the impact of changes in the variance of the observed temperature distribution (Hansen et al., 2013; McKinnon et al., 2016; Rhines & Huybers, 2013), and here we show the regions of the world where such a change in the shape of the temperature is actually affecting temperature extremes.

Quantifying the effectiveness of shifting the temperature distribution by annual mean warming better identifies parts of the world where temperature extremes in any given year are more or less driven by random fluctuations. For large portions of the world (e.g., South America, Africa, Indonesia, and Australia) we show that the number of extremely warm days in a given year is largely related to the annual-mean warming. By elucidating the mechanisms driving changes in the spatiotemporal structure of extreme temperatures, this study contributes to a deeper understanding of the impacts of anthropogenic climate change.

Data Availability Statement

Berkeley Earth Daily Maximum Temperature Data by decade can be found at the following location: https://berkeley-earth-temperature.s3.us-west-1.amazonaws.com/Global/Gridded/Complete_TMAX_Daily_LatLong1_YYYY.nc, where YYYY is the start of a decade such as 1950, 1960, 1970, etc.

ECMWF ERA5 reanalysis data is available at Hersbach et al. (2023).

References

Caesar, J., Alexander, L., & Vose, R. (2006). Large-scale changes in observed daily maximum and minimum temperatures: Creation and analysis of a new gridded data set. *Journal of Geophysical Research*, *111*(D5), D05101. https://doi.org/10.1029/2005jd006280

Coumou, D., & Robinson, A. (2013). Historic and future increase in the global land area affected by monthly heat extremes. *Environmental Research Letters*, *8*(3), 034018. https://doi.org/10.1088/1748-9326/8/3/034018

Diffenbaugh, N. S., & Field, C. B. (2013). Changes in ecologically critical terrestrial climate conditions. *Science*, *341*(6145), 486–492. https://doi.org/10.1126/science.1237123

Donat, M. G., & Alexander, L. V. (2012). The shifting probability distribution of global daytime and night-time temperatures. *Geophysical Research Letters*, *39*(14), L14707. https://doi.org/10.1029/2012gl052459

Fischer, E. M., & Knutti, R. (2014). Detection of spatially aggregated changes in temperature and precipitation extremes. *Geophysical Research Letters*, *41*(2), 547–554. https://doi.org/10.1002/2013gl058499

Hansen, J., Sato, M., & Ruedy, R. (2013). Reply to Rhines and Huybers: Changes in the frequency of extreme summer heat. *Proceedings of the National Academy of Sciences of the United States of America*, *110*(7), E547–E548. https://doi.org/10.1073/pnas.1220916110

Hawkins, E., Frame, D., Harrington, L., Joshi, M., King, A., Rojas, M., & Sutton, R. (2020). Observed emergence of the climate change signal: From the familiar to the unknown. *Geophysical Research Letters*, *47*(6), e2019GL086259. https://doi.org/10.1029/2019gl086259

Hersbach, H., Bell, B., Berrisford, P., Biavati, G., Horányi, A., Muñoz Sabater, J., et al. (2023). ERA5 hourly data on single levels from 1940 to present [Dataset]. *Copernicus Climate Change Service (C3S) Climate Data Store (CDS)*. https://doi.org/10.24381/CDS.ADBB2D47

Hersbach, H., Bell, B., Berrisford, P., Hirahara, S., Horányi, A., Muñoz-Sabater, J., et al. (2020). The ERA5 global reanalysis. *Quarterly Journal of the Royal Meteorological Society*, *146*(730), 1999–2049. https://doi.org/10.1002/qj.3803

Intergovernmental Panel on Climate Change (IPCC). (2023). *Climate change 2022 – impacts, adaptation and vulnerability: Working group ii contribution to the sixth assessment report of the intergovernmental panel on climate change*. Cambridge University Press. https://doi.org/10.1017/9781009325844

Iturbide, M., Gutiérrez, J. M., Alves, L. M., Bedia, J., Cerezo-Mota, R., Cimadevilla, E., et al. (2020). An update of IPCC climate reference regions for subcontinental analysis of climate model data: Definition and aggregated datasets. *Earth System Science Data*, *12*(4), 2959–2970. https://doi.org/10.5194/essd-12-2959-2020

King, A. D., Donat, M. G., Fischer, E. M., Hawkins, E., Alexander, L. V., Karoly, D. J., et al. (2015). The timing of anthropogenic emergence in simulated climate extremes. *Environmental Research Letters*, *10*(9), 094015. https://doi.org/10.1088/1748-9326/10/9/094015

Lau, N.-C., & Nath, M. J. (2012). A model study of heat waves over North America: Meteorological aspects and projections for the twenty-first century. *Journal of Climate*, *25*(14), 4761–4784. https://doi.org/10.1175/jcli-d-11-00575.1

Linz, M., Chen, G., & Hu, Z. (2018). Large-scale atmospheric control on non-Gaussian tails of midlatitude temperature distributions. *Geophysical Research Letters*, *45*(17), 9141–9149. https://doi.org/10.1029/2018gl079324

Loikith, P. C., & Neelin, J. D. (2015). Short-tailed temperature distributions over North America and implications for future changes in extremes. *Geophysical Research Letters*, *42*(20), 8577–8585. https://doi.org/10.1002/2015gl065602

McKinnon, K. A., Rhines, A., Tingley, M. P., & Huybers, P. (2016). The changing shape of northern hemisphere summer temperature distributions. *Journal of Geophysical Research: Atmospheres*, *121*(15), 8849–8868. https://doi.org/10.1002/2016jd025292

McKinnon, K. A., Simpson, I. R., & Williams, A. P. (2024). The pace of change of summertime temperature extremes. *Proceedings of the National Academy of Sciences of the United States of America*, *121*(42), e2406143121. https://doi.org/10.1073/pnas.2406143121

Moore, F. C., Obradovich, N., Lehner, F., & Baylis, P. (2019). Rapidly declining remarkability of temperature anomalies may obscure public perception of climate change. *Proceedings of the National Academy of Sciences of the United States of America*, *116*(11), 4905–4910. https://doi.org/10.1073/pnas.1816541116

Perkins-Kirkpatrick, S. E., & Gibson, P. B. (2017). Changes in regional heatwave characteristics as a function of increasing global temperature. *Scientific Reports*, *7*(1), 12256. https://doi.org/10.1038/s41598-017-12520-2

Perkins-Kirkpatrick, S. E., & Lewis, S. C. (2020). Increasing trends in regional heatwaves. *Nature Communications*, *11*(1), 3357. https://doi.org/10.1038/s41467-020-16970-7

Rhines, A., & Huybers, P. (2013). Frequent summer temperature extremes reflect changes in the mean, not the variance. *Proceedings of the National Academy of Sciences of the United States of America*, *110*(7), E546. https://doi.org/10.1073/pnas.1218748110

Rohde, R. A., & Hausfather, Z. (2020). The Berkeley earth land/ocean temperature record. *Earth System Science Data*, *12*(4), 3469–3479. https://doi.org/10.5194/essd-12-3469-2020

Rohde, R. A., Muller, R., Jacobsen, R., Perlmutter, S., & Mosher, S. (2013). Berkeley earth temperature averaging process. *Geoinformatics & Geostatistics: An Overview*, *1*(2). https://doi.org/10.4172/2327-4581.1000103

Schneider, T., Bischoff, T., & Płotka, H. (2015). Physics of changes in synoptic midlatitude temperature variability. *Journal of Climate*, *28*(6), 2312–2331. https://doi.org/10.1175/jcli-d-14-00632.1

Schneider, T., & Held, I. M. (2001). Discriminants of twentieth-century changes in earth surface temperatures. *Journal of Climate*, *14*(3), 249–254. https://doi.org/10.1175/1520-0442(2001)014<0249:LDOTCC>2.0.CO;2

Simolo, C., Brunetti, M., Maugeri, M., & Nanni, T. (2011). Evolution of extreme temperatures in a warming climate. *Geophysical Research Letters*, *38*(16), L16701. https://doi.org/10.1029/2011gl048437

Simolo, C., & Corti, S. (2022). Quantifying the role of variability in future intensification of heat extremes. *Nature Communications*, *13*(1), 7930. https://doi.org/10.1038/s41467-022-35571-0

Weaver, S. J., Kumar, A., & Chen, M. (2014). Recent increases in extreme temperature occurrence over land. *Geophysical Research Letters*, *41*(13), 4669–4675. https://doi.org/10.1002/2014gl060300

Wills, R. C., Schneider, T., Wallace, J. M., Battisti, D. S., & Hartmann, D. L. (2018). Disentangling global warming, multidecadal variability, and El Niño in pacific temperatures. *Geophysical Research Letters*, *45*(5), 2487–2496. https://doi.org/10.1002/2017gl076327